

Indiana U. Task D Note
3 π Note - 001
Issued: 15 October 2004
Revised: February 8, 2005

Preparing the E852 $\pi^-p \rightarrow \pi^+\pi^-\pi^-p$ and $\pi^-p \rightarrow \pi^-\pi^0\pi^0p$ data samples.*

Ryan Mitchell
Department of Physics
Indiana University, Bloomington, IN 47405

Abstract

This note describes the preparation of the E852 $\pi^-p \rightarrow \pi^+\pi^-\pi^-p$ and $\pi^-p \rightarrow \pi^-\pi^0\pi^0p$ data samples, including a brief description of the E852 detector, and discussion of the trigger, event selection criteria, kinematic fitting, and analysis cuts.

*Work supported by Department of Energy contract DE-FG02-91ER40661.

1 Introduction

This note describes the way the $\pi^-p \rightarrow \pi^+\pi^-\pi^-p$ and $\pi^-p \rightarrow \pi^-\pi^0\pi^0p$ data samples were selected. For convenience, they will be referred to as the “charged” and “neutral” modes, respectively. From a physics point of view, the two modes complement each other nicely, providing cross-checks between different decay sequences. For example, assuming the conservation of isospin, an $X^- \rightarrow \rho^0\pi^- \rightarrow \pi^+\pi^-\pi^-$ decay sequence in the charged mode will be accompanied by an equal amount of the $X^- \rightarrow \rho^-\pi^0 \rightarrow \pi^-\pi^0\pi^0$ decay sequence in the neutral mode. Similarly, there should be twice as many $X^- \rightarrow f\pi^- \rightarrow \pi^+\pi^-\pi^-$ reactions in the charged mode as there are $X^- \rightarrow f\pi^- \rightarrow \pi^0\pi^0\pi^-$ reactions in the neutral mode.

The two reactions also complement each other from an experimental point of view, providing cross-checks of experimental systematics. The two modes come from different triggers: the charged mode from the “133” trigger and the neutral from the “111” trigger, which will be explained in section 3. Furthermore, measuring the charged mode relies entirely on the charged particle tracking, while the neutral mode utilizes the Lead Glass Detector (LGD) to measure the two neutral pions. Any misunderstandings of the experimental acceptance, then, could potentially show up as inconsistencies in physics results between the charged and neutral modes.

While the $\pi^-p \rightarrow \pi^+\pi^-\pi^-p$ and $\pi^-p \rightarrow \pi^-\pi^0\pi^0p$ reactions are measured differently in the detector, the cuts used to reject background share many features. Both data samples can be improved by kinematic fitting and a subsequent confidence level cut, by requiring the event vertex is within the target region, by requiring the parameters of the missing recoiling proton are consistent with detector responses in the central barrel region, and so on. For this reason, the data samples will be developed side by side in this note, even though in practice they were studied independently. Before describing the cuts, however, a brief overview of the E852 detector will be given.

2 The E852 Experiment and Detector

The $\pi^-p \rightarrow \pi^+\pi^-\pi^-p$ and $\pi^-p \rightarrow \pi^-\pi^0\pi^0p$ data samples were taken by the E852 Collaboration during the 1995 running period. The E852 detector (figure 1) used a hydrogen target and sat at the end of an 18.3 GeV/c momentum π^- beam originating from protons at the Alternating Gradient Synchrotron (AGS) at Brookhaven National Laboratory (BNL). The detector was a major upgrade to the already existing Multi Particle Spectrometer (MPS). Details of the beamline and detector can be found in reference [1]. This section will merely list aspects of the detector that are essential for the 3π analyses.

The π^- beam had an average momentum of 18.3 GeV/c, momentum bite $\Delta p/p$ of 3%, and momentum resolution $\delta p/p$ of approximately 1%. The cylindrical liquid hydrogen target was ≈ 30 cm long with a diameter of ≈ 6 cm.

In the forward region, charged particle tracking was done using a series of six drift chambers and three proportional wire chambers (TPX-1, TPX-2, TPX-3) in a 1 T magnetic field. The first two wire chambers (TPX-1 and TPX-2) were also used for triggering. A Lead Glass Detector (LGD),

BNL Experiment E852
A Search for Mesons with Unusual Quantum Numbers

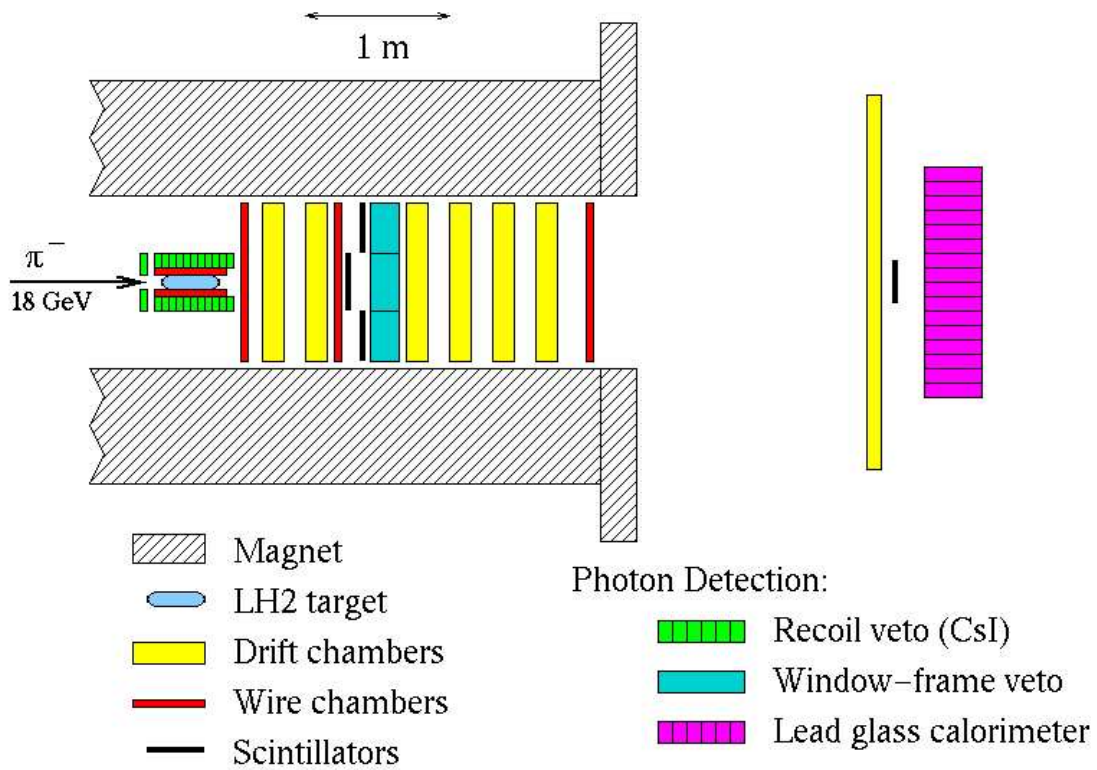


Figure 1: The E852 detector.

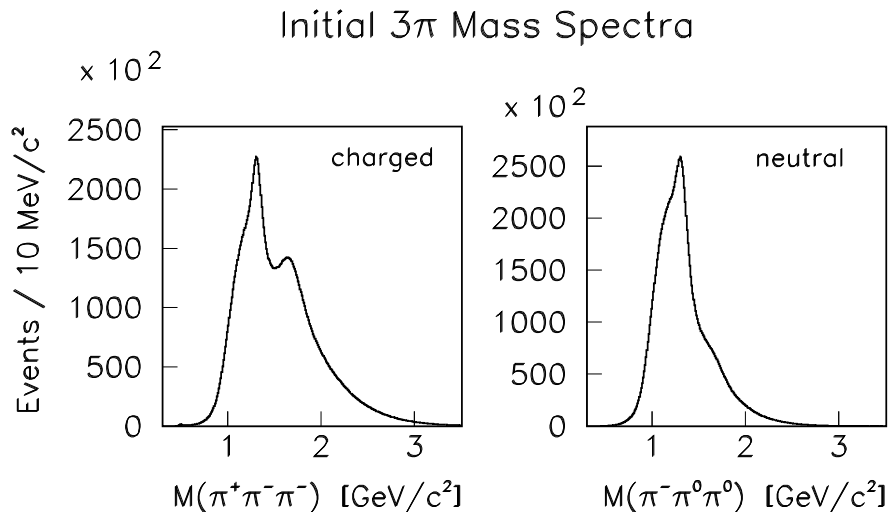


Figure 2: The initial $\pi^+\pi^-\pi^-$ and $\pi^-\pi^0\pi^0$ mass spectra. This is before full kinematic fitting and before any higher level cuts. The π^0 mass was constrained in the neutral mode.

consisting of ≈ 3000 4×4 cm lead glass blocks arranged in a 284×172 cm rectangular array, was used to reconstruct photons. Forward photons outside the acceptance of the LGD could be vetoed by the lead/scintillator Downstream Endcap Array (DEA), marked in figure 1 as the “window-frame veto” (see section 8).

In the central region, the direction of the recoiling proton was measured with a cylindrical wire chamber (TCYL). In final states where a recoiling proton is required (such as the $\pi^-p \rightarrow \pi^+\pi^-\pi^-p$ and $\pi^-p \rightarrow \pi^-\pi^0\pi^0p$ reactions), TCYL was a part of the trigger. Events with central photons were vetoed using a cylindrical CsI calorimeter.

3 Initial Samples

The first step in preparing the $\pi^-p \rightarrow \pi^+\pi^-\pi^-p$ and $\pi^-p \rightarrow \pi^-\pi^0\pi^0p$ data samples was to select initial samples. The initial $\pi^-p \rightarrow \pi^+\pi^-\pi^-p$ data sample comes from the “133” trigger with the requirement that no photons are reconstructed in the LGD. The initial $\pi^-p \rightarrow \pi^-\pi^0\pi^0p$ data sample, on the other hand, is the output of the “111” trigger with the additional requirement that four photons are reconstructed.

3.1 $\pi^-p \rightarrow \pi^+\pi^-\pi^-p$

The $\pi^-p \rightarrow \pi^+\pi^-\pi^-p$ data sample originates with the “133” level-1 trigger – meaning one track was found in the central TCYL drift chamber (presumably the proton), and three charged tracks were in coincidence in the forward TPX-1 and TPX-2 proportional wire chambers (presumably the

Initial 2π Mass Spectra

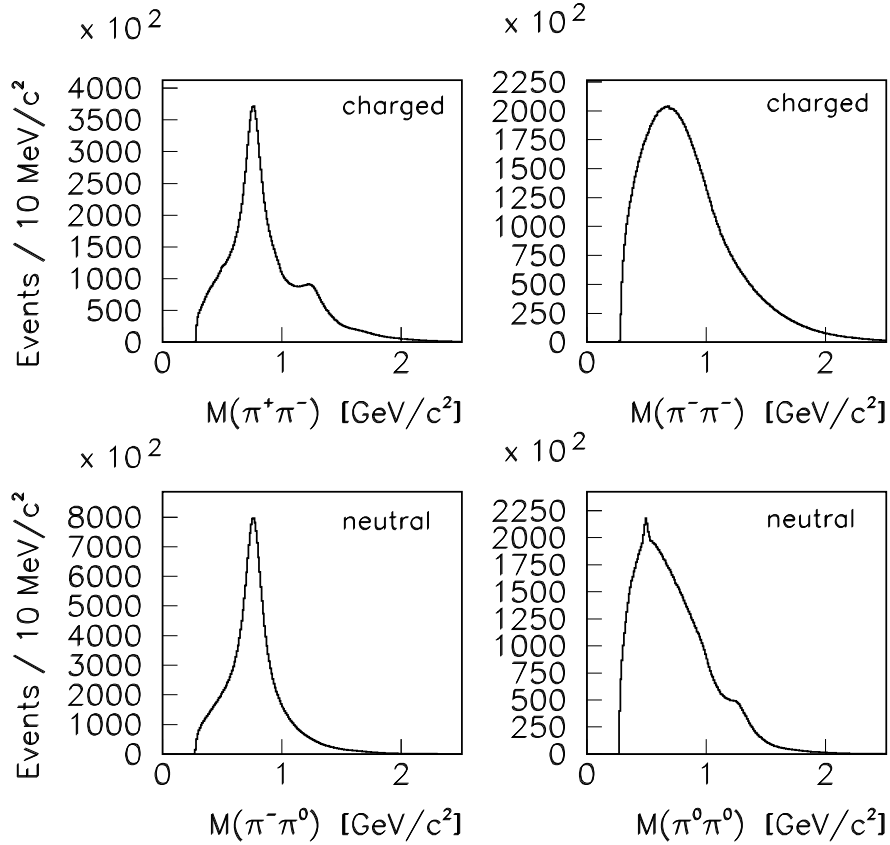


Figure 3: The initial 2π mass spectra from the charged and neutral modes. The upper left plot is $M(\pi^+\pi^-)$ (where one of the two π^- in the reaction has been chosen randomly); the upper right is $M(\pi^-\pi^-)$; the lower left is $M(\pi^-\pi^0)$ (with two entries per event); and the lower right is $M(\pi^0\pi^0)$. As in figure 2, this is before full kinematic fitting and before any higher level cuts. Again, the π^0 mass was constrained in the neutral mode.

π^0 Signal Before Constrained Fit

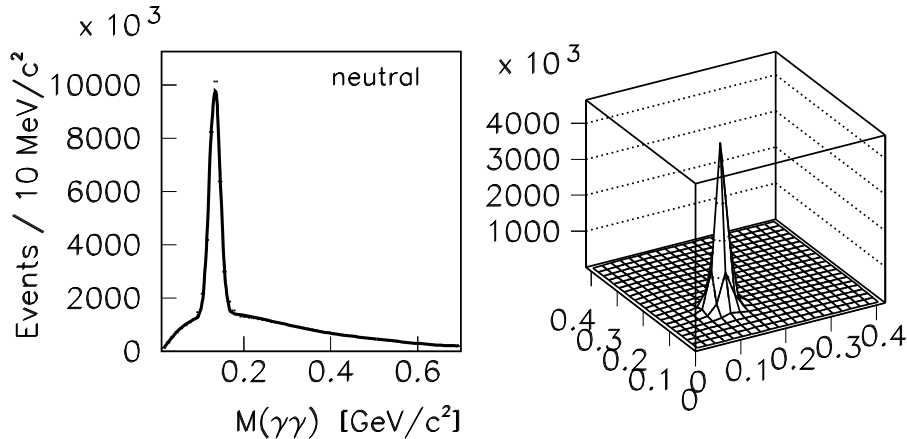


Figure 4: The initial 2γ mass spectrum before any kinematic fitting and before any higher level cuts. The left plot includes all six $\gamma\gamma$ possibilities; the right includes all three $\gamma\gamma$ vs $\gamma\gamma$ possibilities (the x and y axes chosen randomly).

three pions). The 133 level-1 output was then passed through the level-2 trigger where the total photon mass was required to be above $200\text{MeV}/c^2$, biasing the sample against single π^0 's (which, of course, is irrelevant for an all charged particle reaction). A total of 78,659,511 events satisfied this combination of level-1 and level-2 triggers. Of these events, 16,796,457 satisfied the requirement that no photons are reconstructed in the LGD. This data set is what we refer to as the “initial sample” of $\pi^-p \rightarrow \pi^+\pi^-\pi^-p$ events.

An idea of the quality of the initial sample can be given by the 3π and 2π mass distributions. Figure 2 shows the 3π mass distribution (including all 16,796,457 events), in which clear $a_2(1320)$ and $\pi_2(1670)$ peaks can be seen. Figure 3 shows the $\pi^+\pi^-$ and $\pi^-\pi^-$ mass distributions for the same data sample. The $\pi^+\pi^-$ distribution shows a clean sample of the $\rho(770)$ as well as the $f_2(1270)$. As expected, the $\pi^-\pi^-$ distribution has no structure.

3.2 $\pi^-p \rightarrow \pi^-\pi^0\pi^0p$

The $\pi^-p \rightarrow \pi^-\pi^0\pi^0p$ data sample, on the other hand, is derived from the “111” level-1 trigger, which required one track in the central TCYL (presumably the proton) and one track in coincidence in the TPX-1 and TPX-2 wire chambers (presumably the charged pion). After passing the 111 trigger, the total photon mass was required to be above $200\text{MeV}/c^2$ in the level-2 trigger. There were 123,748,800 events satisfying these requirements. Of these, 13,737,265 survived the requirement that four photons were reconstructed in the LGD. This is the “initial sample” of $\pi^-p \rightarrow \pi^-\pi^0\pi^0p$ events.

The $\gamma\gamma$ mass distribution, including all six $\gamma\gamma$ combinations from four photons, is shown in figure 4

Confidence Level Cut

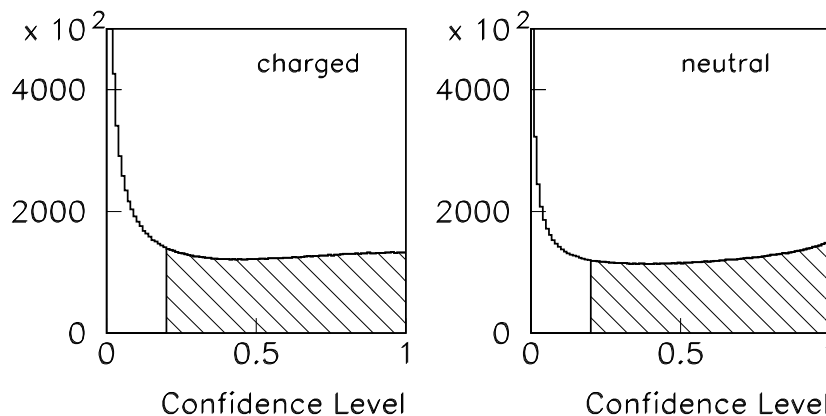


Figure 5: The confidence level cut. The shaded region is the region kept after requiring $C.L. > 20\%$. The left plot is for the $\pi^-p \rightarrow \pi^+\pi^-\pi^-p$ data set; the right is for the $\pi^-p \rightarrow \pi^-\pi^0\pi^0p$ data set.

before any constraints were applied to the π^0 mass. Fitting the mass distribution with a Gaussian and a polynomial background, the $\gamma\gamma$ peak was found to have a mass of $132.7 \text{ MeV}/c^2$ and width $12.3 \text{ MeV}/c^2$. Also shown in figure 4 is a plot of $M(\gamma\gamma)$ vs. $M(\gamma\gamma)$, which includes all three possible ways to form two $\gamma\gamma$ combinations from four photons. A very clean signal peak can be seen corresponding to the simultaneous production of two π^0 's.

For the sake of making figures, the two $\gamma\gamma$ combinations closest to the π^0 mass within an event were constrained to have come from π^0 's. Figure 2 shows the total 3π mass (including all 13,737,265 events) with this π^0 constraint. As in the case of the charged mode, clear $a_2(1320)$ and $\pi_2(1670)$ peaks can be seen. Figure 3 shows the $\pi^-\pi^0$ (one entry for each π^0) and $\pi^0\pi^0$ mass distributions for the same data sample. The $\pi^-\pi^0$ distribution shows a clean sample of the $\rho^-(770)$ and the $\pi^0\pi^0$ distribution shows the $f_2(1270)$. The $\pi^0\pi^0$ distribution also shows a signal of K_S events, which will gradually weaken as cuts are applied (see section 12).

4 The Kinematic Fit and Confidence Level Cut (for both charged and neutral modes)

The first step in processing the initial sample was to do a kinematic fit in conjunction with a confidence level cut. For the charged mode data set, the program SQUAW [2] was used to constrain the missing mass – that is, all track momenta in the final state were perturbed within their errors subject to the constraint that the missing mass is equal to the mass of the proton. In the neutral mode data set, SQUAW also perturbed the photon measurements subject to the π^0 mass constraint. Events emerging from these fits with a low confidence level are likely to be poorly measured events; or they could be background events, such as events with a missing track or events including a

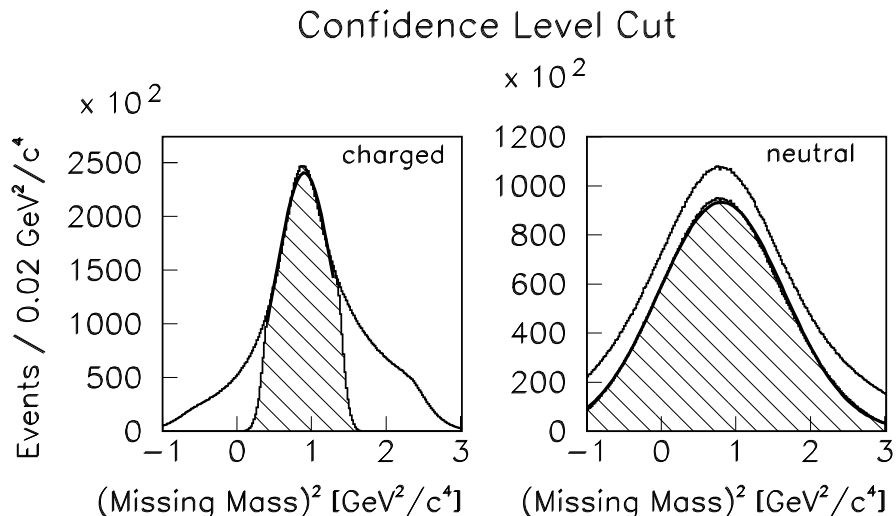


Figure 6: Missing mass squared before and after the confidence level cut. The left plot is for the charged mode, where the confidence level cut effectively limits the range of the missing mass distribution. The right plot is for the neutral mode. Both histograms have been fit with a Gaussian.

$K_S \rightarrow \pi\pi$ decay (see the very small enhancement in the $M(\pi^+\pi^-)$ distribution of figure 3 and the more prominent enhancement in $M(\pi^0\pi^0)$).

4.1 $\pi^-p \rightarrow \pi^+\pi^-\pi^-p$

Figure 5 shows the confidence level distribution with a cut at 20%. This cut value eliminates the excess of events with low confidence level; beyond the 20% line, the confidence level distribution is reasonably flat. The 20% confidence level cut takes the data sample from 16,796,457 to 10,157,455 events. (A 10% cut would leave 11,742,604 events, roughly 15% more than the 20% cut.)

The effect of the confidence level cut on the missing mass squared distribution can be seen in figure 6. Since there is only one constraint in the kinematic fit – the proton mass – the confidence level cut essentially tightens the missing mass squared distribution around the proton mass squared ($0.880 \text{ GeV}^2/c^4$). The 20% confidence level cut brings the high end of the missing mass squared spectrum down to around $1.5 \text{ GeV}^2/c^4$, which is approximately the $\Delta(1232)$ mass squared. Thus, baryon resonances that decay completely to unmeasured particles (that is, particles that end up as part of the missing momentum) are suppressed.

Fitting the missing mass squared distribution between 0.3 and $1.4 \text{ GeV}^2/c^4$ with a Gaussian (shown in figure 6), the mean is found to be $0.904 \text{ GeV}^2/c^4$ (slightly higher than the ideal $0.880 \text{ GeV}^2/c^4$ of the proton) and the width is $0.380 \text{ GeV}^2/c^4$. After subsequent cuts (as will be shown), the mean becomes closer to its nominal value and the width narrows.

Figure 7 shows the $\pi^+\pi^-\pi^-$ mass distribution before and after the kinematic fit and confidence

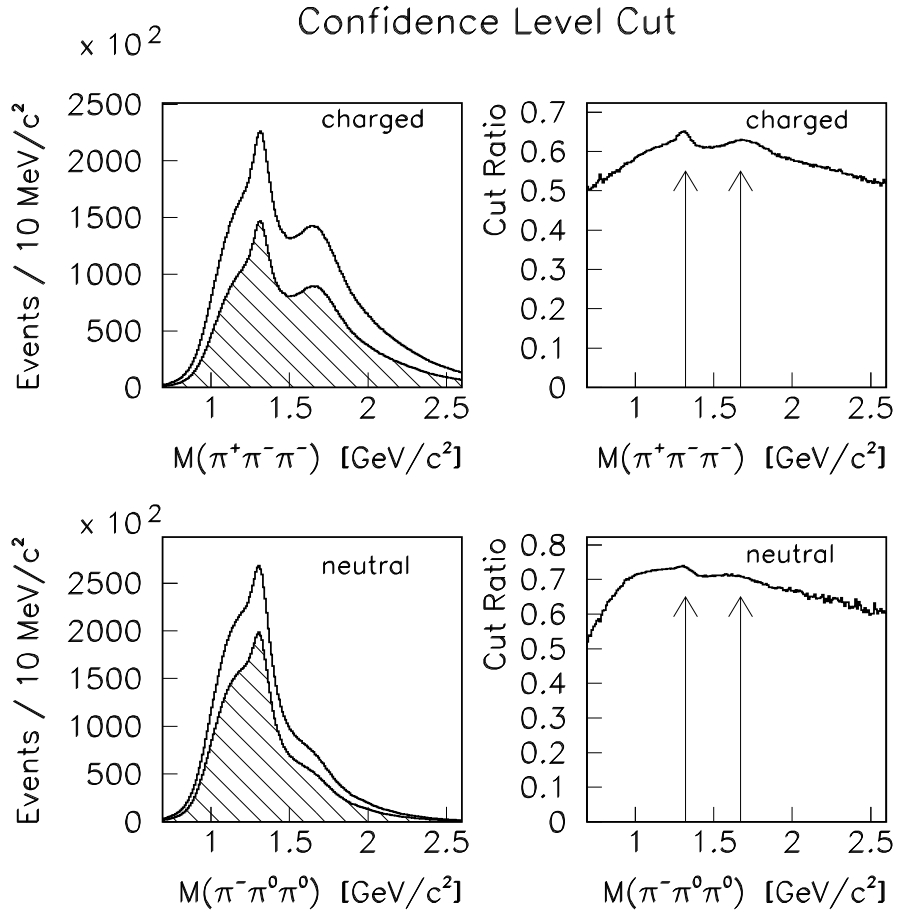


Figure 7: The $M(3\pi)$ mass spectra before and after the confidence level cut. The top two plots are for the charged mode; the bottom two for the neutral mode. The right plots are ratios of before and after showing the effect of the confidence level cut. The arrows are at $1320 \text{ MeV}/c^2$ and $1670 \text{ MeV}/c^2$, showing the effects of the cuts on the $a_2(1320)$ and the $\pi_2(1670)$, respectively.

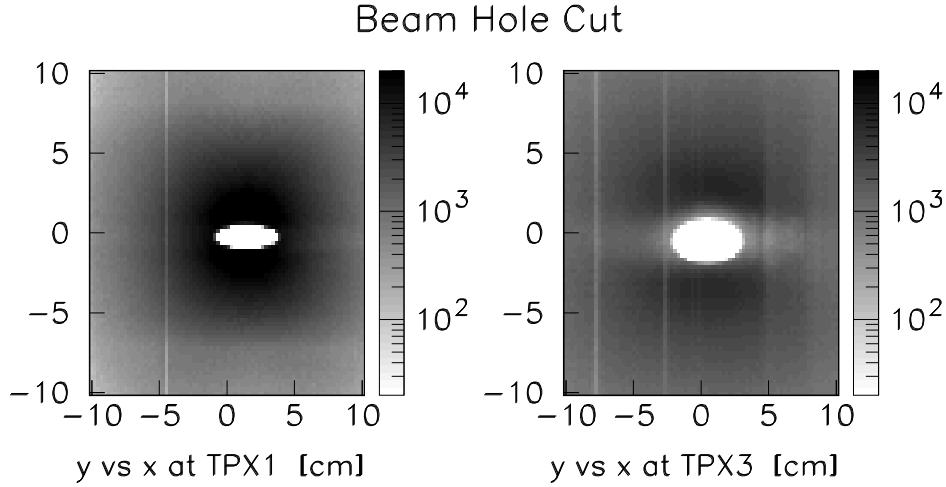


Figure 8: Hits at the TPX1 and TPX3 tracking chambers after a beam hole cut has been applied. The distributions are taken from the $\pi^-p \rightarrow \pi^+\pi^-\pi^-p$ reaction. The neutral mode is very similar.

level cut. The ratio of before and after shows that both the $a_2(1320)$ and $\pi_2(1670)$ signals have been enhanced.

4.2 $\pi^-p \rightarrow \pi^-\pi^0\pi^0p$

A confidence level cut of 20% was also used in the neutral mode. The confidence level distribution above 20% is slightly less uniform than in the charged mode (see figure 5), possibly indicating some slight misunderstanding of the LGD resolution, but it is certainly reasonable. The 20% confidence level cut reduces the data sample from 13,737,265 to 9,813,524 events.

Figure 6 shows the effect of the confidence level cut on the missing mass squared distribution. The distribution is wider for the neutral mode than the charged mode because of the poorer resolution of the neutral pions compared to the charged pions. Furthermore, the confidence level cut does not tighten the missing mass as much as in the case of the charged mode because of the additional constraints on the π^0 mass in the kinematic fit (i.e., the kinematic fit does more than just constrain the proton mass). Fitting the resulting distribution with a Gaussian, we find a mean of $0.809 \text{ GeV}^2/c^4$ (slightly less than the ideal $0.880 \text{ GeV}^2/c^4$) and a width of $0.845 \text{ GeV}^2/c^4$.

Figure 7 shows the $\pi^-\pi^0\pi^0$ mass distribution before and after the kinematic fit and confidence level cut. The ratio of before and after shows that both the $a_2(1320)$ and $\pi_2(1670)$ signals have been enhanced, although not as dramatically as in the charged mode.

5 The Beam Hole Cut (for both charged and neutral modes)

Because of some run-dependent inefficiencies in the center of the TPX1 and TPX3 tracking chambers around the non-interacting beam trajectory, events with tracks going through these regions were cut. This greatly improves our understanding of the acceptance without substantially hurting the statistics. To implement the cut, the average pion beam direction was traced through the magnetic field to the z positions of the TPX1 and TPX3 chambers. Using the errors on the pion beam momentum, a 2.5σ region around the beam was defined in each chamber. Events with charged tracks entering this area were cut. Figure 8 shows the front face of the TPX1 and TPX3 chambers (y vs x) after the cut was imposed on the charged mode data set. The cut was applied in the same way to the neutral mode data set.

Of the 10,157,455 $\pi^- p \rightarrow \pi^+ \pi^- \pi^- p$ events satisfying the confidence level cut, 8,038,452 survived the beam hole cut. A smaller percentage of the neutral mode data set was cut since there is only one charged particle compared to three. The $\pi^- p \rightarrow \pi^- \pi^0 \pi^0 p$ data set went from 9,813,524 to 9,406,003 events.

The effects of this cut (and all subsequent cuts) on 3π mass and missing mass squared can be found in figures 19 to 22. Tabulations of statistics are included in tables 1 and 2 of section 11.

6 The Vertex Cut (for both charged and neutral modes)

The next step was to require that the event vertex fall within the target region. Along the z direction (the beam direction), the E852 target extends from 162 to 192 cm. We restricted the event vertex for both the charged and neutral mode data sets to the range between 163 and 191 cm, which leaves 1 cm of room on either end of the target. In addition, the transverse position of the vertex was required to be within 2.5σ of the nominal beam position, resulting in an elliptical cut. The resulting z and y versus x vertex positions can be seen in figure 9.

One positive byproduct of this cut is to eliminate an enhancement in small $\pi^+ \pi^- \pi^-$ mass. (Note how small this enhancement is to begin with, however, compared to the approximately 10 million events in the total distribution). The vertex cut completely eliminates this effect, as shown in figure 10.

Another positive effect is to reduce K_S contamination. Figure 3 shows some very small hint of a K_S signal in $\pi^+ \pi^-$, and a much stronger signal in $\pi^0 \pi^0$. The confidence level cuts eliminate much of the K_S ; and after the vertex cuts it is completely gone in the charged mode, and greatly reduced in the neutral mode. (See figure 25 for the 2π masses after all cuts have been applied, and section 12 for a discussion of K_S contamination.)

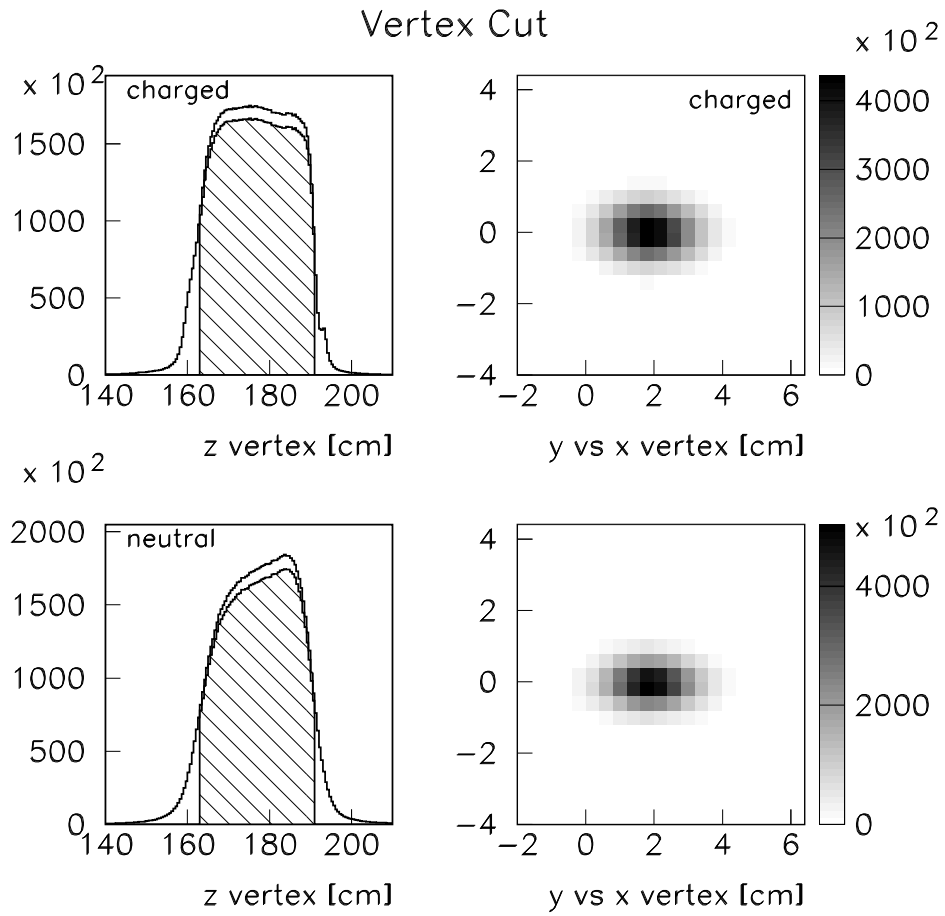


Figure 9: The vertex cut. The top two plots are for the charged mode; the bottom two for the neutral mode. The left plots show the z vertex distribution before and after the vertex cuts. The right plots are the y vs x vertex distributions after the cuts.

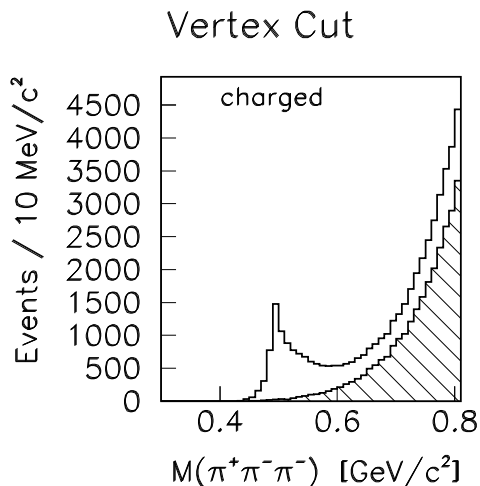


Figure 10: Low $\pi^+\pi^-\pi^-$ mass events. One byproduct of the vertex cut is to eliminate an extraneous enhancement at low $\pi^+\pi^-\pi^-$ mass.

7 The Recoiling Proton Cuts (for both charged and neutral modes)

Ideally, the $\pi^-p \rightarrow \pi^+\pi^-\pi^-p$ reaction results in a central-going recoil proton and three forward-going pions. Similarly, the $\pi^-p \rightarrow \pi^-\pi^0\pi^0p$ reaction should result in a central-going recoil proton and one forward-going pion. As discussed earlier, the trigger required that there is one charged track hitting the central TCYL, and assumed that this track would be the proton. To reinforce our interpretation of these events, we can make sure this track was the proton by imposing two cuts[†].

The first cut requires that the azimuthal angle of the TCYL hit be within 20 degrees of the azimuthal angle of the proton (actually the missing momentum) projected through the magnetic field to the TCYL position. The left plots of figure 11 show the definite correlation between $\phi(\text{missing momentum})$ and $\phi(\text{TCYL})$; and the right plots show the difference between the two azimuthal angles.

The most noticeable effect of this cut is to reduce an anomalous enhancement at low- t (and low missing momentum)[‡]. This is shown in figure 12. After the cut, there is still some residual anomalous behavior at low- t .

The second requirement on the recoiling proton is to guarantee that the proton has a high enough momentum to make it out of the hydrogen target. For every event, the distance the proton traveled through the hydrogen was calculated using the vertex position and the direction of the missing momentum. This distance was compared to a table of proton ranges through hydrogen. After this

[†]Technically, this step could be taken at the time of the kinematic fitting. To simplify the kinematic fit, however, we only required the missing mass be equal to the proton mass, regardless of the resulting direction of the proton momentum.

[‡]We define t as $t \equiv -(P_{beam} - P_{3\pi})^2$, where P_{beam} and $P_{3\pi}$ are the 4-momenta of the beam and 3π systems, respectively, so that t is always positive.

Proton Azimuthal Angle Cut

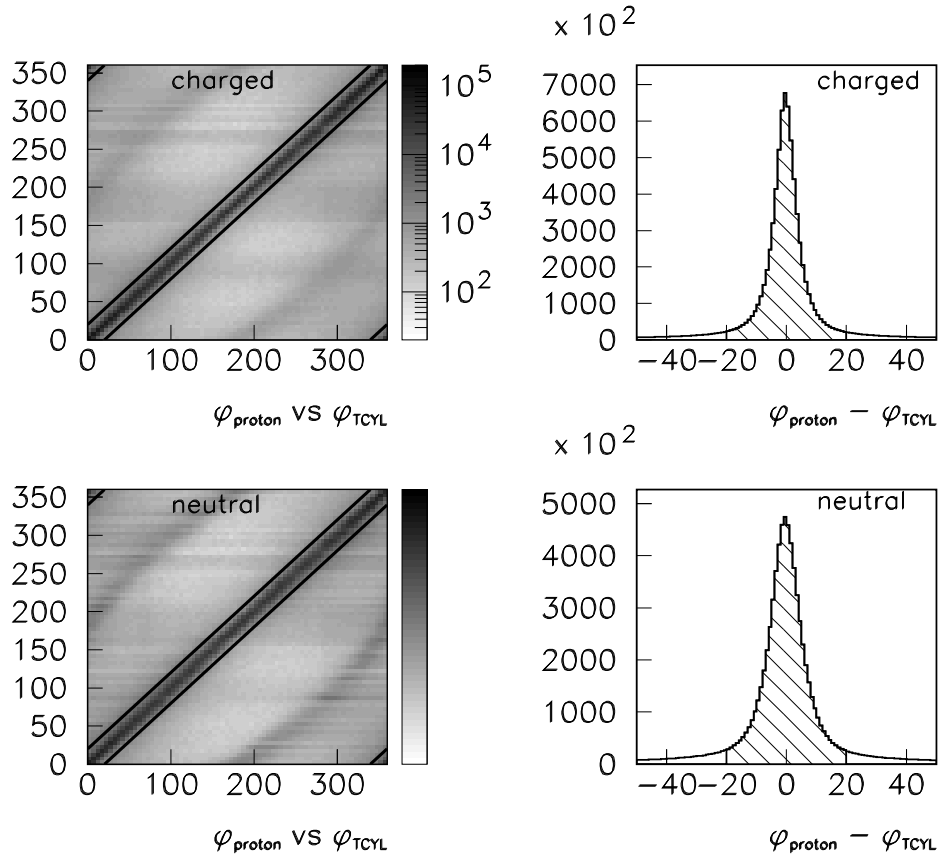


Figure 11: The azimuthal angle cut. The top two plots are for the charged mode; the bottom two for the neutral mode. The left plots show the angle of the proton track (the missing momentum direction) versus the angle of a hit in TCYL. The solid lines indicate the regions where the two angles are within 20 degrees. The right plots show histograms of the azimuthal angle differences, with the 20 degree cuts shaded.

Proton Azimuthal Angle Cut

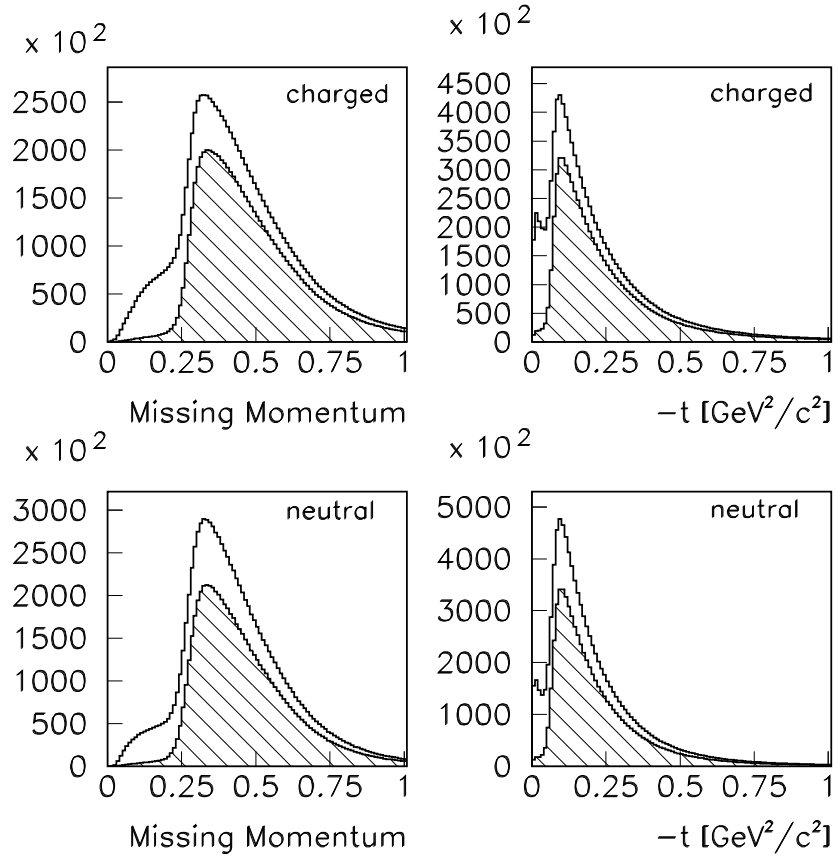


Figure 12: The missing momentum (left plots) and t distributions (right plots) before and after the azimuthal angle cut. The top two plots are for the charged mode; the bottom two for the neutral mode.

Proton Range + Azimuthal Angle Cut

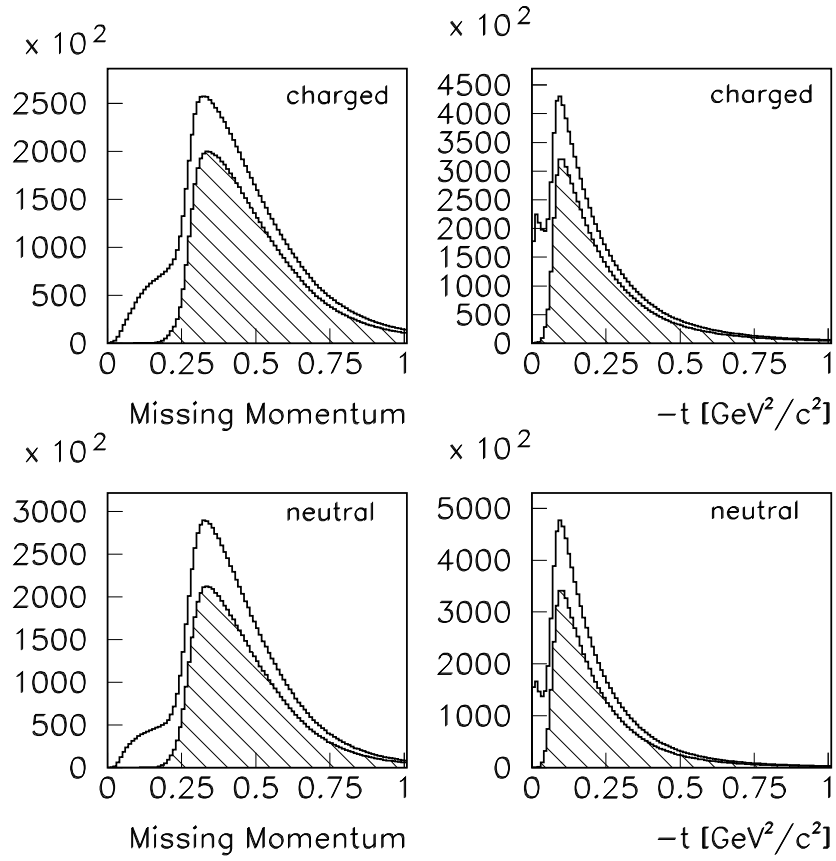


Figure 13: Same as figure 12 except a proton range cut has been added. Now the anomaly at low- t (and low missing momentum) is completely gone.

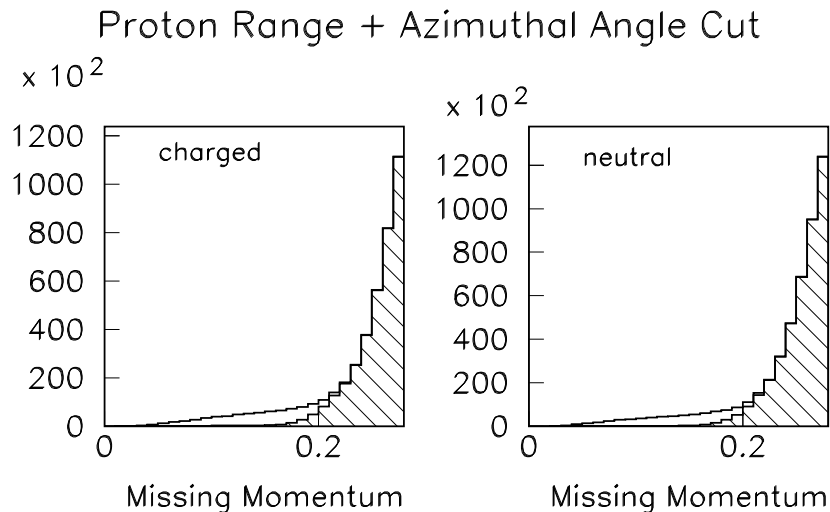


Figure 14: The shaded regions are the missing momenta after the azimuthal angle cuts and the proton range cuts; the unshaded regions only implement the azimuthal angle cuts. The figures show the beneficial effect of the proton range cuts. The left plot is the charged mode; the right the neutral mode.

additional cut, all anomolous behavior in t and missing momentum is gone, as is shown in figure 13.

Another important effect of the recoiling proton cuts is to smooth out the $p\pi$ mass distributions. Figure 14 shows that some previous irregularities are nearly gone after the azimuthal angle and proton range cuts are applied.

8 The CsI and DEA Cuts (for both charged and neutral modes)

When selecting the initial samples of events, it was required that either no photons are reconstructed in the LGD (the charged mode) or four photons are reconstructed (the neutral mode). More stringent selections can be imposed by the additional requirements that no photons are detected in either the CsI (covering the central region) or the DEA (covering the forward region outside the acceptance of the LGD). This reduces events with stray photons, which could originate from misidentified events or could potentially come from unwanted baryon resonances.

The CsI cut was made on the untagged energy (i.e., the energy not associated with a charged track) detected in the CsI detector. The CsI detector was a barrel calorimeter with 18 azimuthal segmentations and 10 longitudinal segmentations resulting in 180 total CsI crystals. It surrounded the TCYL drift chamber so that charged particles could be easily tagged. The untagged energy was required to be less than 20 MeV (figure 16).

To detect photons in the angular region between the central CsI detector and the forward LGD, the DEA (Downstream Endcap Array) detector was used. The DEA consisted of layers of lead and

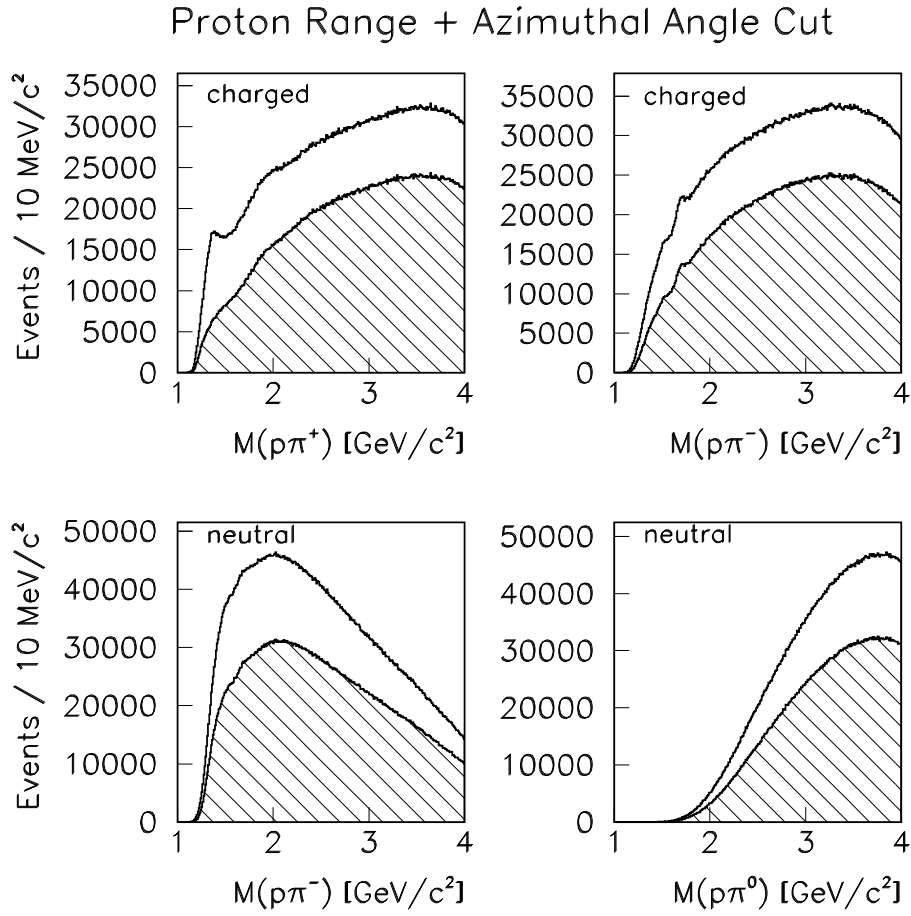


Figure 15: Effects of the recoiling proton cuts on baryon mass combinations: $M(p\pi^+)$ and $M(p\pi^-)$ from the charged mode (top), and $M(p\pi^-)$ and $M(p\pi^0)$ from the charged mode (bottom). The recoiling proton cuts clearly improve the shapes of the $M(p\pi)$ masses.

Untagged CsI Energy Cut

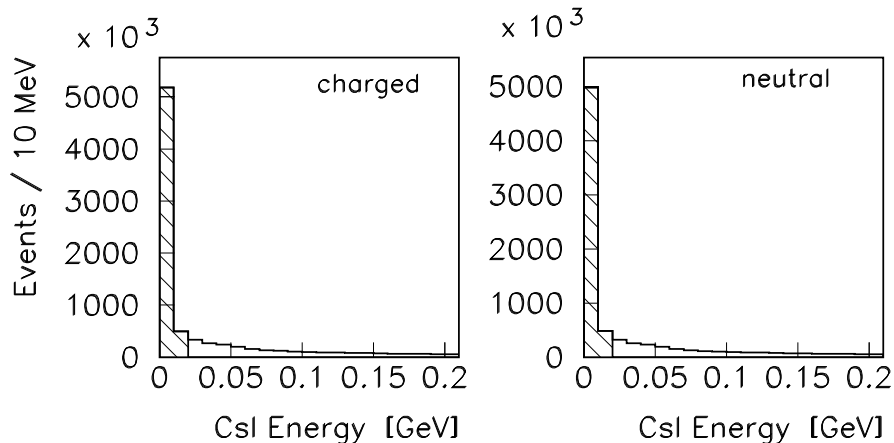


Figure 16: The untagged CsI energy for the charged mode (left) and the neutral mode (right). The shaded region represents the cut at 20 MeV.

scintillator and surrounded the acceptance of the LGD. Charged tracks were detected immediately upstream of the DEA by the CPV (Charged Particle Veto), which was a scintillator detector roughly matching the geometry of the DEA. Events with a signal in the DEA and no signal in the CPV were vetoed, thus eliminating the final class of stray photons.

This combination of cuts takes out roughly half of the events of both the charged and neutral modes. Of the 10,157,455 $\pi^-p \rightarrow \pi^+\pi^-\pi^-p$ events surviving the 20% confidence level cut, 4,822,330 are left after the CsI and DEA cuts. The neutral mode drops from 9,813,524 to 4,939,661 events under the same conditions.

9 A Δ^{++} Cut (for the charged mode only)

After all the above cuts have been imposed, we still notice a small indication of the Δ^{++} in the $p\pi^+$ mass distribution (figure 17). We eliminate this directly by requiring $M(p\pi^+) > 1.5 \text{ GeV}/c^2$. A byproduct of this cut is to remove an enhancement at low π^+ momentum (also shown in figure 17).

The cut has a minor impact on the total number of events: of the 10,157,455 events satisfying the confidence level cut, 9,749,031 survive the Δ^{++} cut. Figure 19 shows that the cut has no major impact on the 3π mass spectrum. The cut also doesn't significantly change the missing mass squared shape (see table 1).

The Δ^{++} Cut (charged mode only)

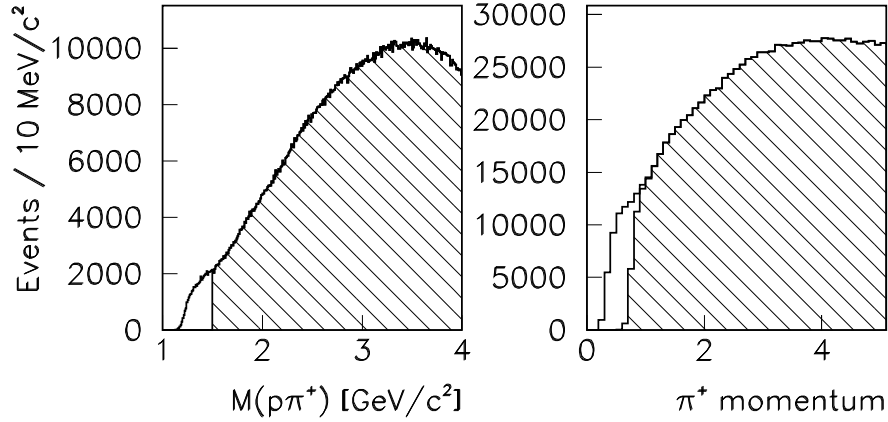


Figure 17: The Δ^{++} Cut. The left plot shows the $M(p\pi^+)$ mass distribution after all cuts have been applied. The indication of a Δ^{++} led to a straightforward cut – $M(p\pi^+) > 1.5 \text{ GeV}/c^2$ – which is also shown in the left plot. The right plot shows the π^+ momentum before and after the Δ^{++} cut.

Photon Separation Cut (neutral mode only)

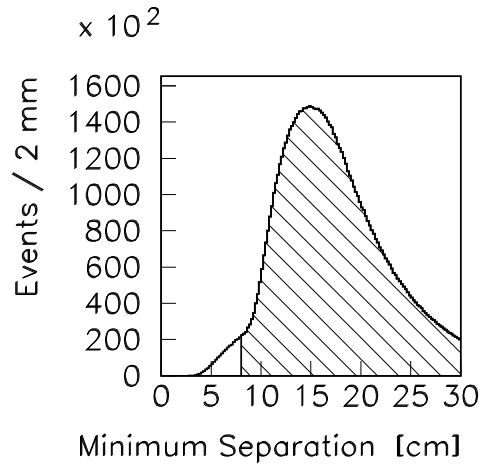


Figure 18: The minimum distance of separation between photons at the surface of the LGD in the $\pi^- p \rightarrow \pi^- \pi^0 \pi^0 p$ reaction. A minimum distance separation of 8 cm was chosen as a cut, as indicated by the shaded region of the figure.

10 Photon Separation Cut (for the neutral mode only)

When reconstructing photons in the LGD, care must be taken to avoid showers that are too close together to be cleanly separated. This concern is easily addressed by requiring a minimum distance of separation between photons incident on the front surface of the LGD. A plot of minimum distance between clusters from the $\pi^-p \rightarrow \pi^-\pi^0\pi^0p$ reaction (figure 18) indicates that the reconstruction becomes idiosyncratic at separations less than around 8 cm. This is a reasonable value since the lead glass block size is 4×4 cm. So, a minimum photon separation cut of 8 cm was applied to the $\pi^-p \rightarrow \pi^-\pi^0\pi^0p$ reaction.

11 Cut Summary

In summary, the final cuts applied to the $\pi^-p \rightarrow \pi^+\pi^-\pi^-p$ and $\pi^-p \rightarrow \pi^-\pi^0\pi^0p$ data sets are:

1. Confidence Level $> 20\%$. (section 4)
2. Beam Hole $> 2.5 \sigma$. (section 5)
3. z Vertex between 163 and 191 cm. (section 6)
4. x,y Vertex within 2.5σ of the target center. (section 6)
5. Azimuthal angle < 20 degrees. (section 7)
6. Proton range cut. (section 7)
7. Untagged CsI energy < 20 MeV. (section 8)
8. No untagged DEA hits. (section 8)
- 9a. $M(p\pi^+) > 1.5 \text{ GeV}/c^2$ (charged mode only). (section 9)
- 9b. Minimum photon separation > 8 cm (neutral mode only). (section 10)

Figures 19 and 21 show the effects of each of the cuts on the 3π mass for the charged and neutral modes, respectively. Figures 20 and 22 show the effects of each of the cuts on the missing mass squared distributions of the two modes.

The effects of all the cuts applied together can be seen in the last figures (bottom left) of figures 19 to 22. The cuts clearly sharpen the 3π mass distribution, and also narrow the missing mass squared distributions.

Table 1 lists some effects of each of the cuts on the $\pi^-p \rightarrow \pi^+\pi^-\pi^-p$ data sample; table 2 lists effects on the $\pi^-p \rightarrow \pi^-\pi^0\pi^0p$ data sample.

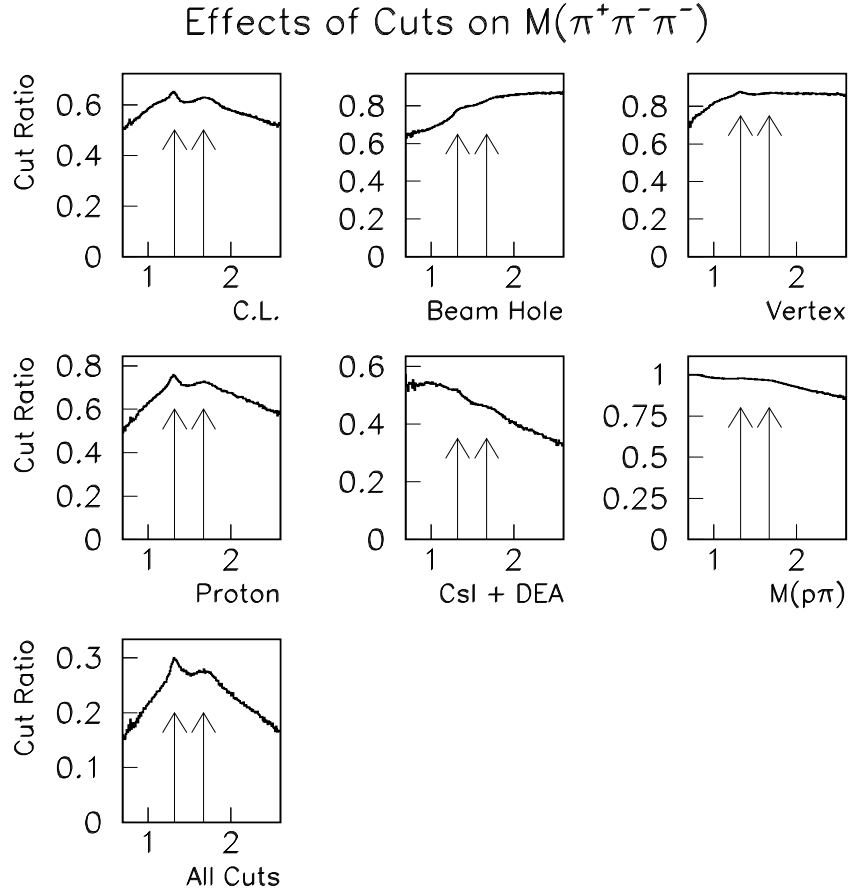


Figure 19: The effects of cuts on $M(\pi^+\pi^-\pi^0)$. The histograms are ratios of $M(\pi^+\pi^-\pi^0)$ before and after the indicated cuts were applied. The confidence level cut (top left) is measured with respect to the initial data sample. All the rest of the ratios are taken with respect to the data sample with only the confidence level cut applied. All cuts are applied individually (except for the plot marked “all cuts”, which has all cuts applied). The two arrows mark 1320 and 1670 MeV/c², indicating the effects of the cuts on the $a_2(1320)$ and $\pi_2(1670)$, respectively.

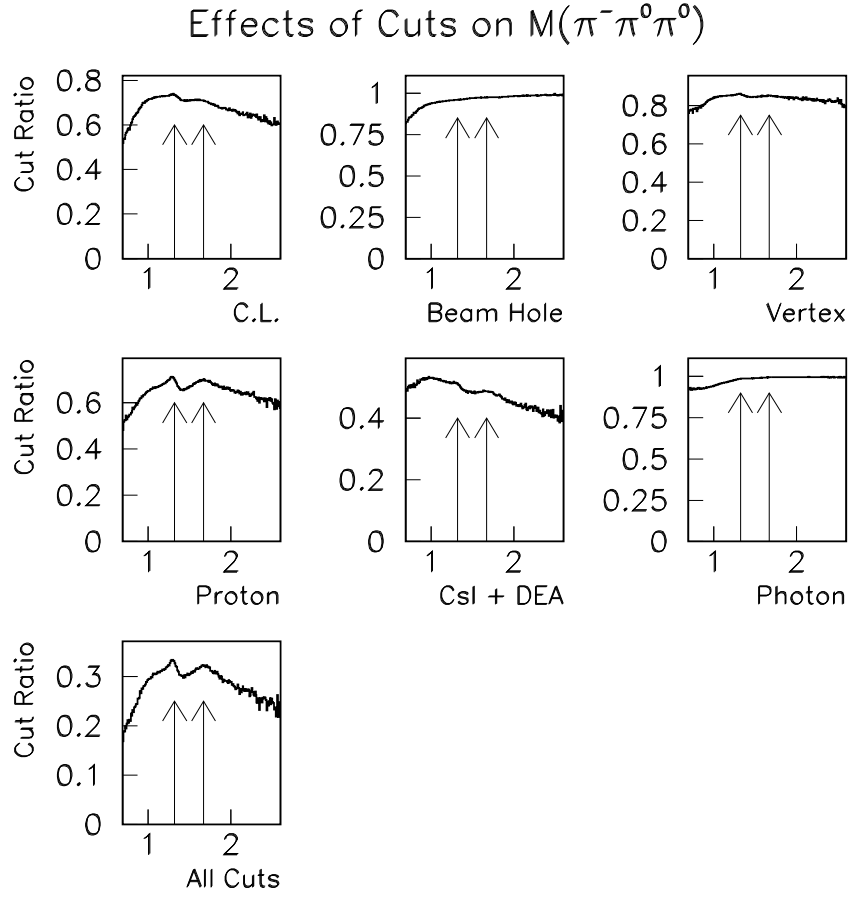


Figure 21: The effects of cuts on $M(\pi^-\pi^0\pi^0)$. The histograms are ratios of $M(\pi^-\pi^0\pi^0)$ before and after the indicated cuts were applied. The confidence level cut (top left) is measured with respect to the initial data sample. All the rest of the ratios are taken with respect to the data sample with only the confidence level cut applied. All cuts are applied individually (except for the plot marked “all cuts”, which has all cuts applied). The two arrows mark 1320 and 1670 MeV/c^2 , indicating the effects of the cuts on the $a_2(1320)$ and $\pi_2(1670)$, respectively.

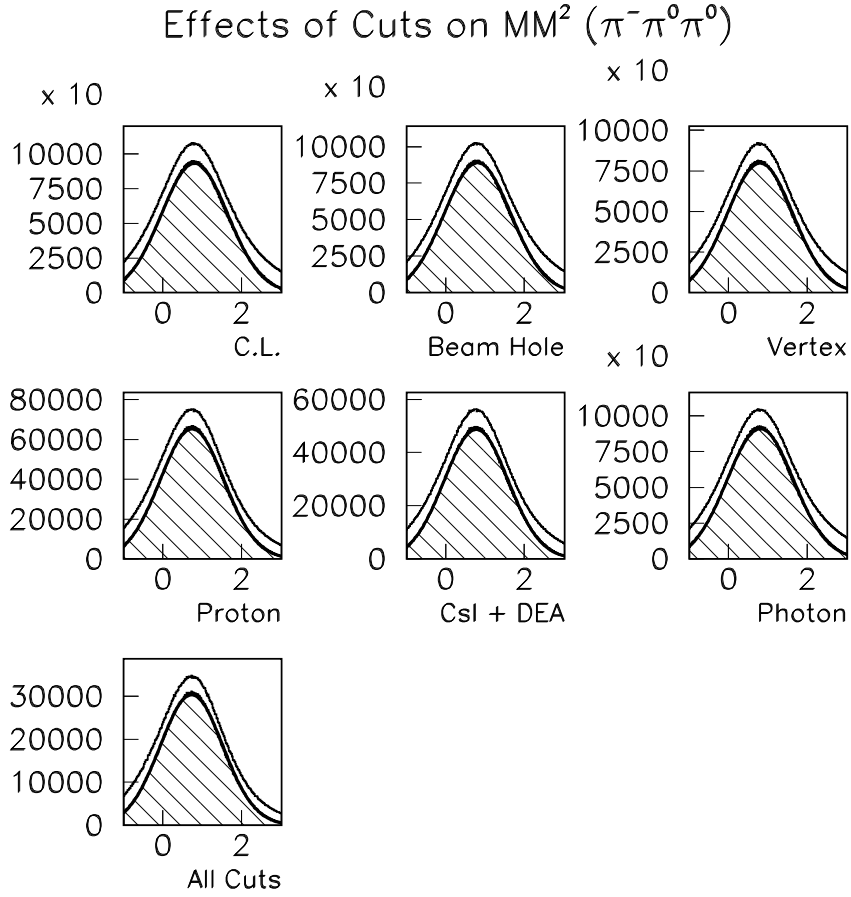


Figure 22: The effects of cuts on the missing mass squared in the $\pi^-p \rightarrow \pi^-\pi^0\pi^0p$ reaction. The confidence level cut (top left) is applied first. Subsequent cuts are applied individually. The unshaded regions are without the confidence level cut, the shaded regions are with the confidence level cut. Each distribution has been fit with a Gaussian between -1.0 and $3.0 \text{ GeV}^2/c^4$. Results are tabulated in table 1.

| | Events | MM^2 Mean | MM^2 Width |
|--|------------|--|--|
| INITIAL CUTS | | | |
| Satisfying 133 Trigger | 78,659,511 | | |
| Require no photons | 16,796,457 | 0.904 GeV ² /c ⁴ | 0.380 GeV ² /c ⁴ |
| Confidence Level Cut | 10,157,455 | 0.904 GeV ² /c ⁴ | 0.380 GeV ² /c ⁴ |
| ADDITIONAL CUTS (applied individually) | | | |
| Beam Hole Cut | 8,038,452 | 0.904 GeV ² /c ⁴ | 0.372 GeV ² /c ⁴ |
| Vertex Cut | 8,723,392 | 0.898 GeV ² /c ⁴ | 0.370 GeV ² /c ⁴ |
| Proton Cuts | 7,030,216 | 0.891 GeV ² /c ⁴ | 0.344 GeV ² /c ⁴ |
| CsI and DEA Cuts | 4,822,330 | 0.891 GeV ² /c ⁴ | 0.352 GeV ² /c ⁴ |
| Δ^{++} Cut | 9,749,031 | 0.907 GeV ² /c ⁴ | 0.375 GeV ² /c ⁴ |
| ALL CUTS | | | |
| Final Sample | 2,585,776 | 0.883 GeV ² /c ⁴ | 0.315 GeV ² /c ⁴ |

Table 1: Summary of cut statistics for the $\pi^- p \rightarrow \pi^+ \pi^- \pi^- p$ data set.

| | Events | MM^2 Mean | MM^2 Width |
|--|-------------|--|--|
| INITIAL CUTS | | | |
| Satisfying 111 Trigger | 123,748,800 | | |
| Require four photons | 13,737,265 | | |
| Confidence Level Cut | 9,813,524 | 0.809 GeV ² /c ⁴ | 0.845 GeV ² /c ⁴ |
| ADDITIONAL CUTS (applied individually) | | | |
| Beam Hole Cut | 9,406,003 | 0.809 GeV ² /c ⁴ | 0.851 GeV ² /c ⁴ |
| Vertex Cut | 8,325,895 | 0.801 GeV ² /c ⁴ | 0.836 GeV ² /c ⁴ |
| Proton Cuts | 6,620,596 | 0.744 GeV ² /c ⁴ | 0.814 GeV ² /c ⁴ |
| CsI and DEA Cuts | 4,939,661 | 0.774 GeV ² /c ⁴ | 0.814 GeV ² /c ⁴ |
| Photon Separation Cut | 9,579,426 | 0.808 GeV ² /c ⁴ | 0.846 GeV ² /c ⁴ |
| ALL CUTS | | | |
| Final Sample | 3,025,981 | 0.731 GeV ² /c ⁴ | 0.801 GeV ² /c ⁴ |

Table 2: Summary of cut statistics for the $\pi^- p \rightarrow \pi^- \pi^0 \pi^0 p$ data set.

12 K_S Contamination

The initial 2π mass spectra, before any cuts were applied, showed signs of K_S contamination (section 3). The effect was most prominent in the $\pi^0\pi^0$ mass distribution. This K_S is most likely a remnant of the $a_2(1320) \rightarrow K^- K_S$ decay and is difficult to completely eliminate from the data sample. Applying all the above cuts, however, does substantially reduce the K_S signal. Figure 23 shows the $\pi^0\pi^0$ mass distributions before and after all the cuts were applied. To enhance the appearance of the K_S the mass plotted is from 4-momenta unperturbed by the global kinematic fit. Only π^0 masses were constrained.

The K_S signals were fit with Gaussians with a polynomial background. Before cuts, the fit returns xxx events out of a total of 13,737,265 events, giving a K_S rate of xxx% of the total events. After

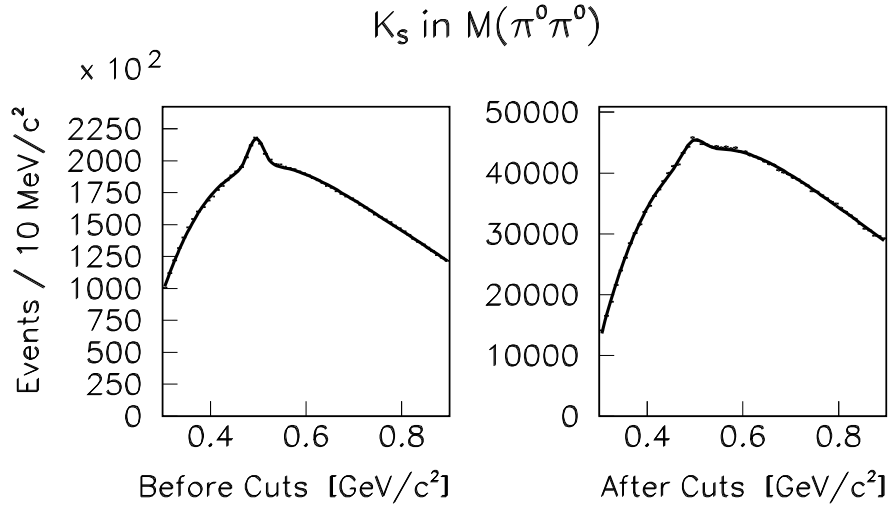


Figure 23: K_S contamination in $\pi^- p \rightarrow \pi^- \pi^0 \pi^0 p$. The left plot shows $M(\pi^0 \pi^0)$ before any cuts were applied; the right plot is after all cuts are applied. The K_S signal is fit with a Gaussian and a polynomial background.

cuts, xxx K_S were found out of a total of 3,025,981 events, a rate of xxx%. Thus, the final data samples contain only a small fraction of events with K_S contamination.

13 A gallery of final distributions

Finally, after all the cuts have been applied, a quick survey of some low level distributions can be made. Figure 24 shows the final 3π masses; figure 25 shows the final 2π mass combinations; figure 26 shows the two $M(p\pi)$ combinations; figure 27 shows the final momentum distributions from the $\pi^- p \rightarrow \pi^+ \pi^- \pi^- p$ reaction; figure 28 shows the final momentum distributions from the $\pi^- p \rightarrow \pi^- \pi^0 \pi^0 p$ reaction; and figure 29 shows the final t distribution.

Final 3π Mass Spectra

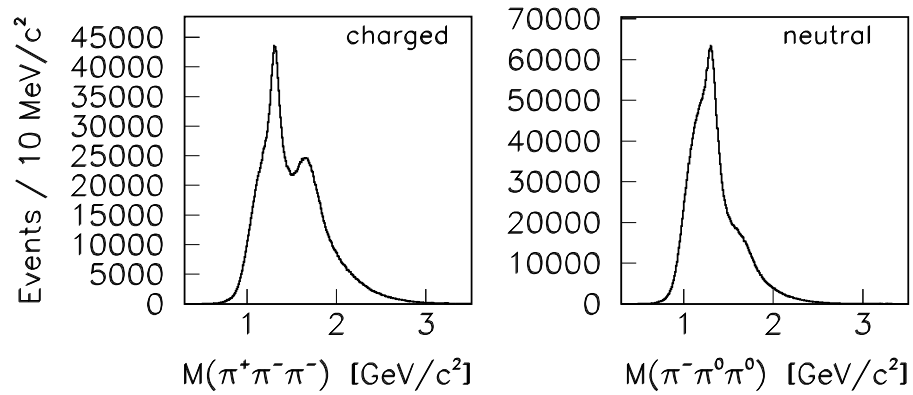


Figure 24: The 3π mass distributions after all of the cuts have been applied. The left is for the charged mode; the right for the neutral mode.

Final 2π Mass Spectra

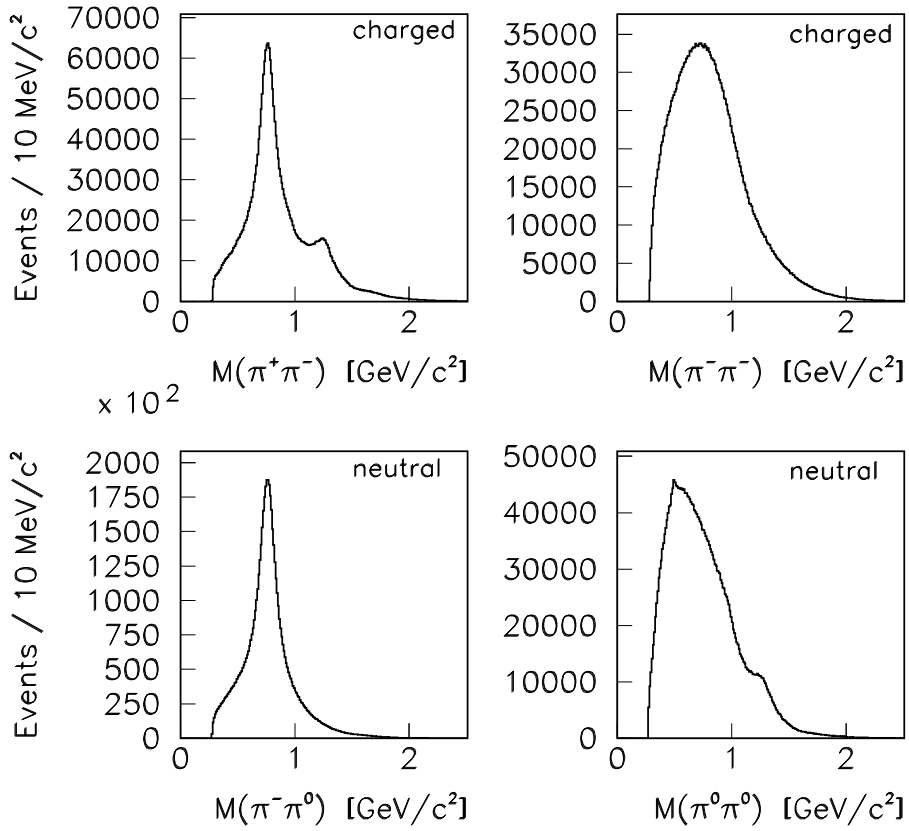


Figure 25: The 2π mass distributions after all the cuts have been applied. Notice the significant weakening of the K_S signal compared to figure 3. The top two are from the charged mode; the bottom two from the neutral mode.

Baryon Combinations

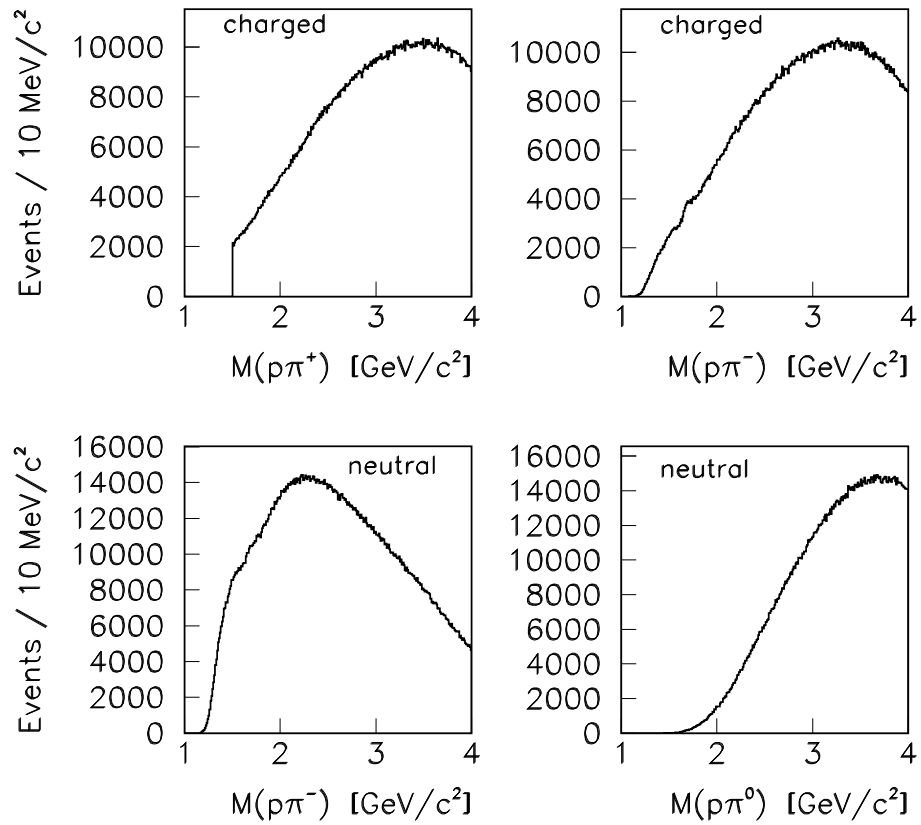


Figure 26: The final $M(p\pi)$ mass distributions. No substantial contamination from baryon resonances can be seen. The top two plots are from the charged mode; the bottom two from the neutral mode.

Momentum Distributions (charged mode)

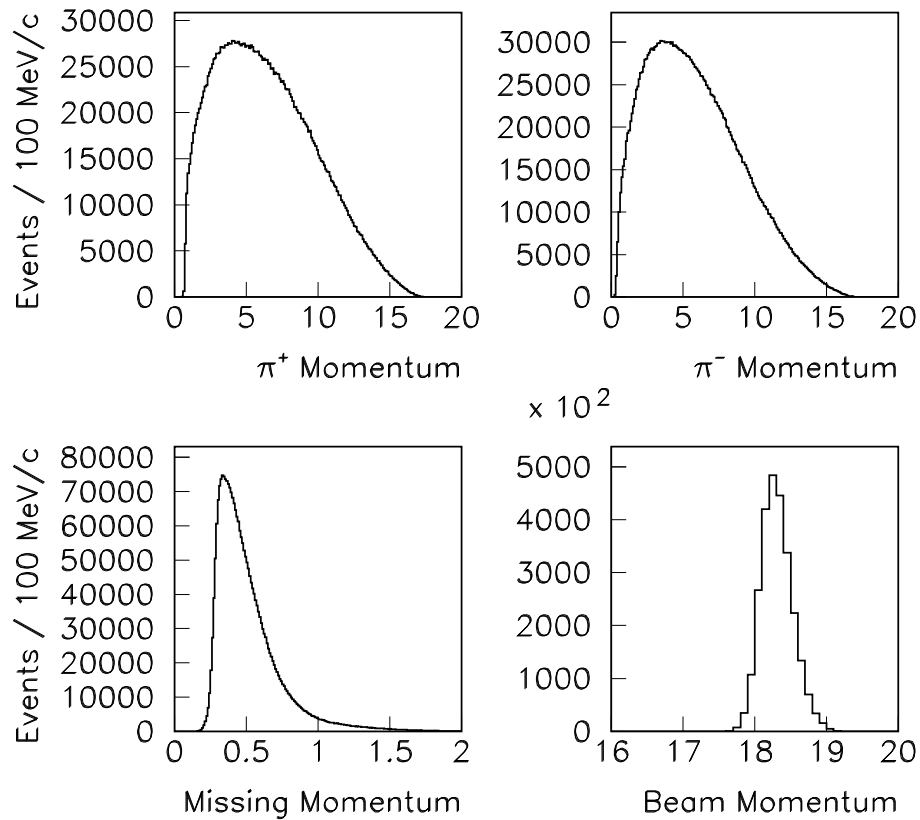


Figure 27: The final momentum distributions from the reaction $\pi^- p \rightarrow \pi^+ \pi^- \pi^- p$. Top left is the π^+ momentum; top right is one of the π^- momenta (the two π^- are symmetric); bottom left is the missing momentum (i.e., the putative proton momentum); bottom right is the measured beam momentum.

Momentum Distributions (neutral mode)

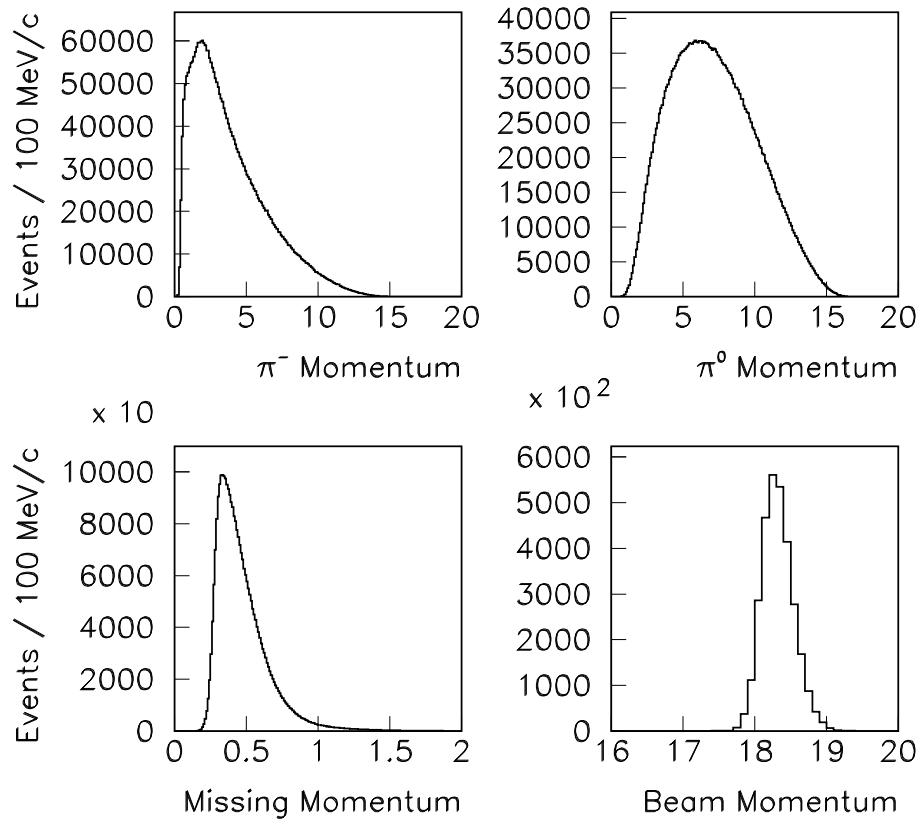


Figure 28: The final momentum distributions from the reaction $\pi^- p \rightarrow \pi^- \pi^0 \pi^0 p$. Top left is the π^- momentum; top right is one of the π^0 momenta (the two π^0 are symmetric); bottom left is the missing momentum (i.e., the putative proton momentum); bottom right is the measured beam momentum.

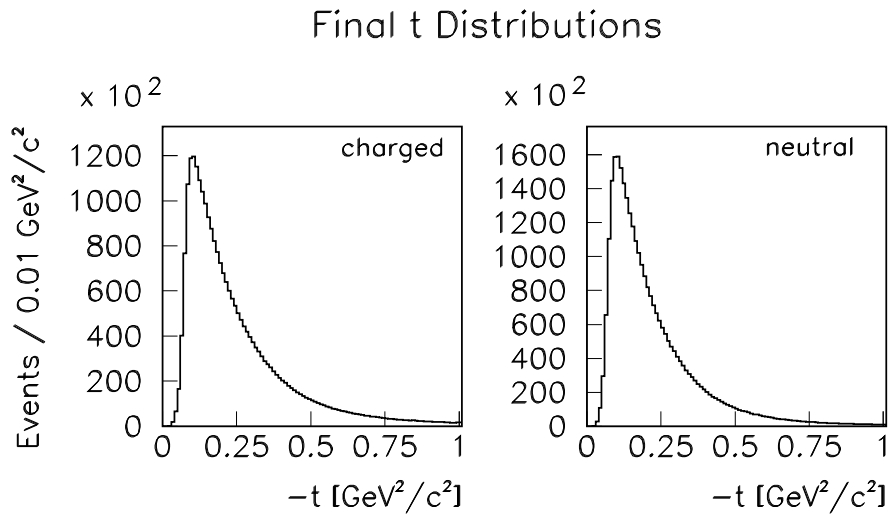


Figure 29: The final t distributions. The left is for the charged mode; the right from the neutral mode.

References

- [1] S. Teige *et al*, Phys. Rev. D. **59**, 012001 (1998).
- [2] squaw reference